Enhanced ordered structure and relaxor behaviour of $0.98Pb(Mg_{1/3}Nb_{2/3})O_3–0.02La(Mg_{2/3}Nb_{1/3})O_3$ single crystals

2008 J. Phys.: Condens. Matter 20 015210

(http://iopscience.iop.org/0953-8984/20/1/015210)

J. Phys.: Condens. Matter **20** (2008) 015210 (7pp) doi:10.1088/0953-8984/20/01/015210

Enhanced ordered structure and relaxor behaviour of $0.98Pb(Mg_{1/3}Nb_{2/3})O_3$–$0.02La(Mg_{2/3}Nb_{1/3})O_3$ single crystals

Xifa Long[1], Alexei A Bokov[1], Zuo-Guang Ye[1], Weiguo Qu[2] and Xiaoli Tan[2]

[1] Department of Chemistry and 4D LABS, Simon Fraser University, Burnaby, BC, V5A 1S6, Canada
[2] Department of Materials Science and Engineering, Iowa State University, Ames, IA 50011, USA

E-mail: zye@sfu.ca

Received 13 August 2007, in final form 23 October 2007
Published 5 December 2007
Online at stacks.iop.org/JPhysCM/20/015210

Abstract

High quality $Pb(Mg_{1/3}Nb_{2/3})O_3$ (PMN) and La-doped PMN (PLMN) single crystals were grown via a top-seeded solution growth method. At a doping level as low as 2 at.% of La, the 1:1 B-site cation (chemical) order was significantly enhanced as revealed by the presence of superlattice peaks in the x-ray diffraction pattern and comparatively large (∼100 nm) chemically ordered regions (CORs) in the transmission electron microscopy dark field images. The average chemical order parameter was calculated (from the intensity of superlattice peaks) to be $S \approx 0.44$. Besides, x-ray diffraction revealed the presence of a low-symmetry (presumably rhombohedral) phase. The effect of La doping on the dielectric relaxation was not substantial. Though the magnitude of the dielectric constant peak in PLMN was reduced by half as compared to pure PMN, the peak temperature and diffuseness as well as the shape of the dielectric relaxation spectra remained almost unchanged. The analysis of the temperature dependence of the characteristic time for the main relaxation process in terms of the Vögel–Fulcher law revealed the freezing of dipole dynamics at temperature $T_f = 192$ K, which was only slightly lower than the $T_f = 213$ K in PMN. To reconcile the structural and dielectric data we suggest that the rhombohedral phase forms inside CORs while the chemically disordered matrix remains cubic and is populated by dynamic polar nanoregions that give rise to the characteristic dielectric response.

1. Introduction

Lead magnesium niobate, $Pb(Mg_{1/3}Nb_{2/3})O_3$ (or PMN), is a prototype relaxor ferroelectric material which features a high maximum value, a broad peak and a strong frequency dispersion of dielectric permittivity as a function of temperature [1, 2]. At room temperature PMN has a cubic ABO_3 perovskite structure, where Pb^{2+} occupies A-sites while Mg^{2+} and Nb^{5+} share the B-sites. The structure involves quenched compositional inhomogeneities in the distribution of the Mg^{2+} and Nb^{5+} cations on the B-sites. Within cation (chemically) ordered regions of a few nanometres in size, the structure adopts a doubled perovskite unit cell due to the $A(B'_{1/2}B''_{1/2})O_3$-type '1:1' ordering with a face centred arrangement of two different (B′ and B″) sublattices [3]. According to the widely accepted random site model [3–5], in PMN the B″ sublattice is occupied solely by Nb^{5+} while the B′ sublattice is occupied by a random 2:1 distribution of Mg^{2+} and Nb^{5+}. These chemically ordered regions (CORs) in which the long-range cation order exists locally are immerged into the chemically disordered matrix in which Mg^{2+} and Nb^{5+} cations are distributed over the B-sites at random so that the long-range order is absent. The CORs as well as the polar nanoregions (PNRs) which persist at temperatures well above the temperature of the dielectric constant maximum T_m are often believed to be the origin

of the characteristic relaxor ferroelectric behaviour [6, 7]. In particular, when analysing the set of known data for the complex lead perovskites, Randall and Bhalla noticed [7] that relaxor behaviour was observed only in those compounds where the nanometre-scale CORs are present. In the materials without mesoscopic inhomogeneities (both chemically fully ordered and fully disordered) the normal ferroelectric or antiferroelectric behaviour was reported. Accordingly, it was suggested that CORs act as sites to localize the dynamic PNRs responsible for the relaxor behaviour. The same conclusion was recently derived theoretically using first-principles-based simulations [8]. However, the direct experimental verification of the spatial correlation between CORs and PNRs is a rather difficult task. Therefore, the investigations in this field can be very helpful for the understanding of the mechanisms of PNR formation and thereby the mechanisms of the relaxor behaviour.

In pure PMN, the size of the CORs was found to be smaller than 5 nm [9, 10]. Growth of these regions by thermal annealing cannot be achieved at temperatures up to 1400 °C [9], which is believed to be due to kinetic rather than thermodynamic constraints [3]. A-site La^{3+}-doping has been found to be an effective way to enhance B-site cation order in PMN [11–14]. The smaller size of La^{3+} than Pb^{2+} and the increased molar fraction of the larger Mg^{2+} cation on the B-site were suggested to account for the enhancement of chemical order [15, 16].

However, almost all studies on doped PMN have been based on polycrystalline bulk ceramics [17, 18]. As a result, dielectric properties cannot be evaluated on specific crystallographic orientations. A recent report found that the orientation dependence of the dielectric/ferroelectric behaviour is strong in pure PMN [19]. Therefore, there is a great need to grow large PMN crystals with various dopants. Although Fanning and co-workers reported the preparation and structure of La-doped PMN crystals [20], their size was small (<1 mm) and the La concentration was comparatively high (4–10%), thus one can expect that not only the characteristics of CORs, but also the La^{3+} cations and associated change of Mg^{2+}/Nb^{5+} ratio, might influence the properties of the crystal. In this work, we have grown La-doped PMN single crystals with 2% of La, investigated the enhancement of the cation ordering by means of x-ray diffraction and transmission electron microscopy dark field imaging and studied the relaxor ferroelectric behaviour.

2. Experimental details

Single crystals of $Pb(Mg_{1/3}Nb_{2/3})O_3$ (PMN) and $0.98Pb(Mg_{1/3}Nb_{2/3})O_3$–$0.02La(Mg_{2/3}Nb_{1/3})O_3$ (PLMN) were grown from high-temperature solution by the top-seeded solution growth (TSSG) method using a home-made tube furnace with controlled temperature gradient field. The La dopant was incorporated through solid solution and the charge neutrality was maintained by adjusting the Mg^{2+}/Nb^{5+} ratio on the B-site. A mixture of PbO and B_2O_3 (with a molar ratio of $PbO:B_2O_3 = 95:5$) was used as flux. The starting chemicals, PbO (99.99%), La_2O_3 (99.99%), MgO (99.9%), Nb_2O_5 (99.9%) and B_2O_3 (99.9%), were weighed according to the stoichiometric composition of PLMN (solute) and the flux to solute molar ratio of 80:20. The weighed chemicals were thoroughly mixed and loaded into a platinum crucible of 50 mm^3 in volume, which was then placed in a vertical tubular furnace. A small PMN single crystal was used as a seed and the saturation temperature of the solution was determined accurately by repeated seeding trials. The saturation temperature indicates the appropriate temperature at which the seed crystal can retain and effectively grow from the solution, i.e. the onset of top-seeded growth. In the trial process, the seed crystal was first preheated above the melt surface for a few minutes before being dipped into the solution. After a period of time, the surface state of the seed was checked to see if it had grown or dissolved. After several experiments, the saturation temperature was determined to be 1148 °C for the PLMN–PbO/B_2O_3 flux system. The crystal growth took place upon cooling from 1150 to 1080 °C at a cooling rate of 0.1 °C h^{-1}. At the end of the slow cooling process, the grown crystal was pulled out of the melt surface and cooled down to room temperature at a rate of 15 °C h^{-1}. Such a process produces PLMN single crystals with dimensions up to $15 \times 15 \times 8$ mm^3.

X-ray powder diffraction was performed on crushed small crystals using a Rigaku *R*-axis diffractometer with Cu Kα radiation. For transmission electron microscopy (TEM) study, fine crystal powder was dispersed in acetone to form a dilute suspension. One droplet of the suspension was dropped onto a copper grid with carbon support film. TEM observation was carried out on a Philips CM30 microscope operated at 300 kV. For dielectric characterization, (100)-oriented crystal platelets of dimensions $\sim 3.5 \times 2.7 \times 0.4$ mm^3 were cut and polished. Then gold layers were sputtered as electrodes. The dielectric permittivity as a function of temperature was measured with a Novocontrol broadband dielectric spectrometer at a series of frequencies upon heating from 150 to 475 K.

3. Results and analysis

3.1. Crystal structure

Figure 1 shows the powder x-ray diffraction pattern of PLMN at room temperature. It can be seen that the pure perovskite phase was preserved. In addition to the major diffraction peaks from the simple perovskite structure, two extra weak peaks appeared at 19.2° and 37.1°, which are shown in the insets of figure 1. These peaks correspond to *d*-spacing values twice those of the (111) and (311) major peaks, respectively. Therefore, these two superlattice peaks can be indexed as (1/2, 1/2, 1/2) and (3/2, 1/2, 1/2), indicating the doubling of the perovskite unit cell due to a strong B-site 1:1 cation order. Calculations of the lattice parameter assuming the cubic symmetry resulted in a value of $a = 4.0298$ Å, which is smaller than that of pure PMN ($a = 4.0477$ Å). The presence of the superlattice peaks (which were not found in the diffraction pattern of pure PMN) and the decrease in lattice parameter firmly indicates that La ions are indeed incorporated into the perovskite lattice.

The chemical order parameter *S* in the PLMN crystals was calculated by dividing the ratio of the experimentally

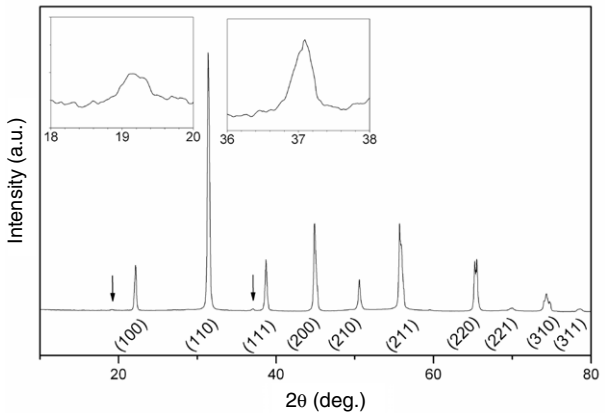

Figure 1. X-ray powder diffraction pattern of the PLMN crystals. Indexing corresponds to the primitive (not doubled) perovskite unit cell.

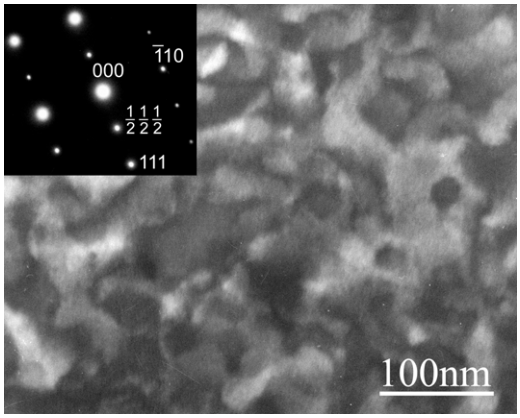

Figure 2. TEM dark field image of the cation ordered chemical domains in the PLMN single crystal. The corresponding electron diffraction pattern with the [112] zone-axis is shown in the inset.

observed superlattice (1/2, 1/2, 1/2) reflection intensity over the fundamental reflection intensity from a parallel plane, (111), by the corresponding calculated ratio for a perfectly ordered sample, that is,

$$S^2 = \frac{\left(\frac{I_{1/2,1/2,1/2}}{I_{111}}\right)_{\rm exp}}{\left(\frac{I_{1/2,1/2,1/2}}{I_{111}}\right)_{S=1}}.$$

The structure of hypothetical perfectly ordered PMN was assumed to be composed of 1:1 ordering of cation $B' = Nb^{5+}$ and complex cation $B'' = (Mg_{2/3}Nb_{1/3})^{3+}$ on the B-site, which gives rise to a superstructure of $Fm3m$ symmetry, while maintaining the charge neutrality [4]. Using the PowderCell program, the x-ray diffraction pattern of the ordered PMN was simulated and thereby the ratio of $I_{1/2,1/21/2}/I_{111}$ was calculated to be 0.0795. The experimental ratio of $I_{1/2,1/21/2}/I_{111}$ for the PLMN crystal was found to be 0.0156 after background subtraction. Therefore, the order parameter S is calculated to be 0.44, i.e. the crystal is far from being completely ordered. On the other hand, the TEM results (see below in this section) suggest considerable spatial inhomogeneity of the ordering degree. Therefore, incomplete chemical ordering may be determined by two factors: coexistence of chemically ordered and disordered regions and incomplete ordering inside CORs ($S = 1$ is theoretically possible only at $T = 0$). The order parameter $S = 0.44$ calculated from x-ray diffraction data represents the average value.

The enhanced chemical order was further confirmed by TEM observations. A fine crystal with its [112] zone-axis close to the incident electron beam was focused. The electron diffraction pattern is shown in the inset of figure 2, where strong (1/2, 1/2, 1/2)-type superlattice diffractions can be noticed. The dark field image formed with the (1/2, 1/2, 1/2) superlattice spot is shown in figure 2. The chemically ordered regions (bright areas) with size up to ∼100 nm are clearly seen. Obviously, 2 at.% La doping already leads to a dramatic increase in the size of the CORs. In ceramics the same size can be obtained only at a much higher La-doping level of ∼10% [4].

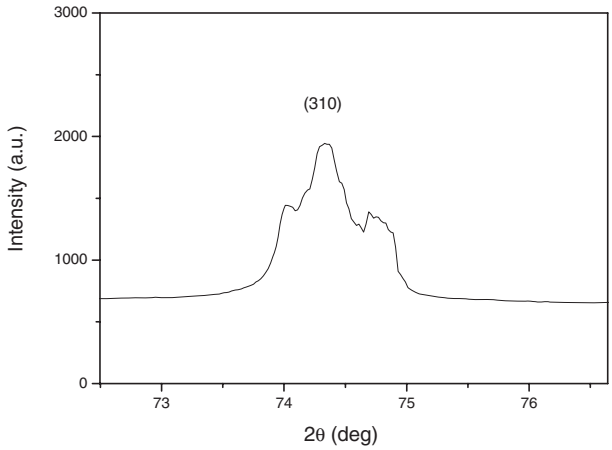

Figure 3. Details of the $(311)_{\rm cub}$ x-ray diffraction peak of PLMN.

The other important difference from PMN is that the x-ray diffraction peaks in PLMN are significantly wider and typically asymmetric or (at large 2θ angles) split, an example of which is shown in figure 3 for the cubic (310) diffraction peak. Such a kind of x-ray diffraction pattern is incompatible with a cubic symmetry. Preliminary phase analysis shows that the structure is composed of a mixture of cubic and rhombohedral phases. It should be noticed that the superlattice reflections are also significantly asymmetric (see the inset in figure 1), which means that the rhombohedral phase exists inside CORs. A conclusion concerning the presence of rhombohedral phase in the chemically disordered regions and the cubic phase in CORs cannot be drawn so far. A more elaborate structural study is underway.

3.2. Dielectric properties

The dielectric constant (ε') and loss ($\tan\delta$) of a (100)-oriented PLMN crystal as a function of temperature at different frequencies (f) are shown in figure 4. It can be seen that a typical relaxor ferroelectric behaviour characteristic of pure PMN is preserved. At 1 kHz, in comparison with a pure PMN

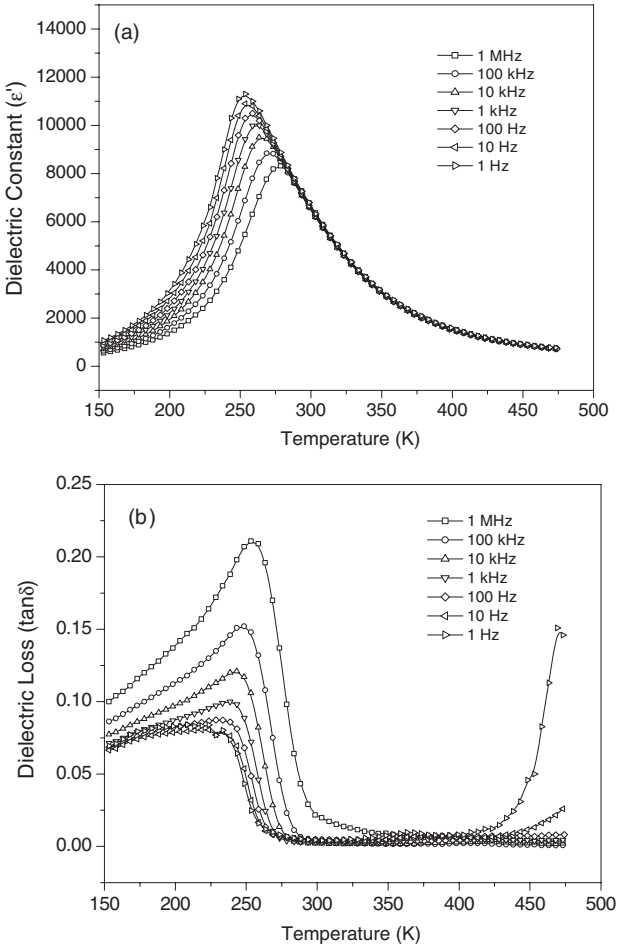

Figure 4. Dielectric constant (a) and loss tangent (b) of the (100)-oriented PLMN crystal as a function of temperature measured at a series of frequencies.

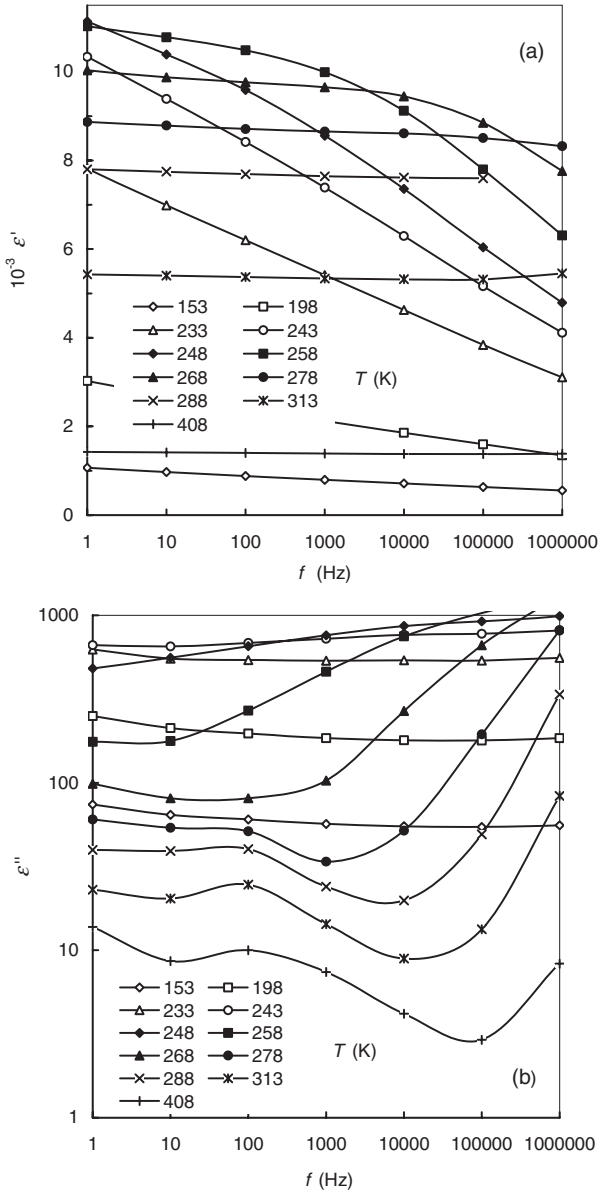

Figure 5. Real (a) and imaginary (b) parts of the dielectric permittivity of the (100)-oriented PLMN crystal as a function of frequency at various temperatures.

single crystal with (100) orientation [19], the ε' maximum decreased from 20×10^3 to 10×10^3 and the corresponding temperature T_m shifted from 268 to 263 K in the PLMN single crystal. This is consistent with the results reported previously [14, 18, 20]. The frequency dependences of the real and imaginary parts of permittivity at selected temperatures are shown in figure 5.

At temperatures above T_m (and below the Burns temperature, T_B), the temperature dependence of ε' in relaxors can be described by a Lorentz-type quadratic relationship [21–23],

$$\frac{\varepsilon_A}{\varepsilon'} - 1 = \frac{(T - T_A)^2}{2\delta^2}, \tag{1}$$

where T_A and ε_A are the fitting parameters and δ is a measure of the degree of diffuseness of the permittivity peak. Figure 6 shows the temperature dependence of $1/\varepsilon'$ for the PLMN crystals above T_m at 100 kHz, which is fitted to this relation. Despite the fact that the magnitude of the $\varepsilon'(T)$ peak in PLMN is half as large as in pure PMN, the diffuseness $\delta = 45$ K is only slightly larger (in the PMN crystal $\delta = 41$ K, in agreement with [22]).

The frequency dependence of the $\varepsilon'(T)$ maximum temperature T_m can be analysed with the empirical Vögel–Fulcher (V–F) relationship [24, 25],

$$f = f_m \exp(E_m/(T_{fm} - T_m)), \tag{2}$$

where f is the measurement frequency and E_m, f_m, and T_{fm} are the parameters. Figure 7 shows the inverse of T_m as a function of f and the related V–F fitting for the PLMN crystal. The maximum temperature derived from the temperature dependences of the imaginary part of the permittivity can also be well fitted to equation (2) in the whole measurement frequency range. The best-fit parameters are listed in table 1 and compared with the parameters for the PMN crystal taken from [26]. It can be seen that doping with 2% La^{3+} ions results in a slightly higher T_{fm} as compared to the pure PMN crystal.

Table 1. Comparison of the relaxation parameters for the PMN and PLMN crystals.

	V–F law for T_m derived from $\varepsilon'(T)$			V–F law for T_m derived from $\varepsilon''(T)$			V–F law for τ		
	f_m (Hz)	E_m (K)	T_{fm} (K)	f_m (Hz)	E_m (K)	T_{fm} (K)	f_0 (Hz)	E_a (K)	T_f (K)
PMN [26]	3×10^{12}	880 ± 30	221.6 ± 0.6	3×10^{12}	860 ± 130	211 ± 3	1×10^{13}	810 ± 60	213 ± 2
PLMN	2.7×10^{12}	750 ± 70	226 ± 1.7	1.1×10^{11}	500 ± 200	221 ± 10	1.4×10^{13}	1080 ± 90	192 ± 8

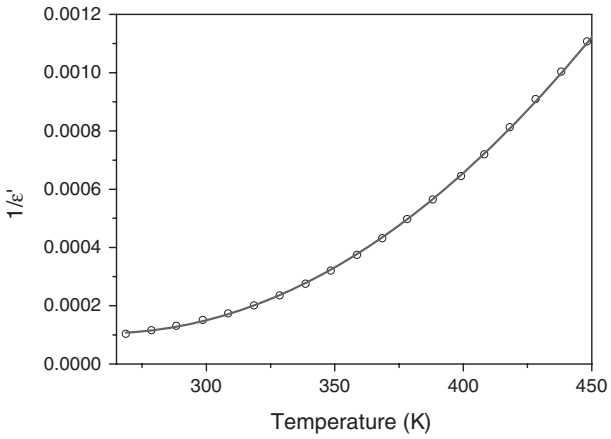

Figure 6. Temperature dependences of $1/\varepsilon'$ of the PLMN single crystals at 100 kHz above T_m (open circles) and the fitting results (line) to the quadratic equation (1) with best-fit parameters $T_A = 257$ K, $\varepsilon_A = 9470$, and $\delta = 45$ K.

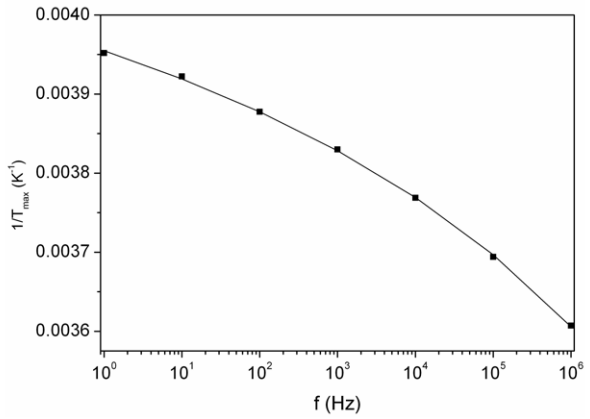

Figure 7. Frequency dependence of T_m (dots) and the fitting result (line) to the V–F law (2) for the PLMN crystal.

In some relaxor ferroelectrics T_{fm} corresponds to the freezing temperature for the dynamics of PNRs due to cooperative interactions between their moments [24–26]. However, satisfaction of relationship (2) does not necessary mean a glassy freezing of dipole dynamics [25]. To confirm the freezing behaviour, the temperature dependence of the corresponding relaxation time should be determined. For this purpose we analyse below the frequency dependences of the permittivity in detail.

The dielectric spectra of PLMN at comparatively lower temperatures (figure 5) are similar to those observed in a pure PMN crystal [26]. Two main relaxation processes can be found in the range of T_m (see e.g. the curve for 268 K in figure 5(b)). The first, so-called universal relaxor (UR), process manifests itself as an increase of ε'' with decreasing f at low frequencies. At higher frequencies the conventional relaxor (CR) relaxation appears as the increase of ε'' with increasing f. Upon cooling the CR dispersion range moves to lower frequencies (this corresponds to an increase of characteristic relaxation time) and disappears from the measurement frequency window at $T \ll T_m$. Frequency-independent losses are observed at low temperatures. Well above T_m an additional relaxation process is found at ~100 Hz, which has not been observed in pure PMN. The strength of this relaxation increases with decreasing T at a much slower rate than the strengths of CR and UR relaxations do, so that at temperatures close to T_m it becomes negligible. This relaxation could result from the effects of La doping in PLMN, the mechanism of which needs further investigation.

Because of the similarity of the relaxation patterns in PLMN and in PMN, we applied for the analysis the same approach that was used in the case of the PMN crystal [26]. The frequency dependences of ε'' and ε' were fitted (simultaneously at each temperature) to the relation

$$\varepsilon^*(f) = \chi_U^*(f) + \chi_R^*(f) + \varepsilon_\infty, \tag{3}$$

where the first two terms are related to the UR and CR contributions, respectively, and ε_∞ originates from other possible polarization processes exhibiting dispersion above the upper limit of the measurement frequency window. To describe the CR contribution we used the Kohlrausch–Williams–Watts (KWW) relaxation pattern, the shape of which in the time domain is described by the stretched exponential function, $\exp[-(t/\tau)^\beta]$. The UR contribution was expressed as

$$\chi_U'(f) = \chi_{U1} f^{n-1}$$

$$\chi_U''(f) = \cot(n\pi/2)\chi_{U1} f^{n-1}.$$

The adjustable parameters used in the course of the nonlinear least-square fitting procedure were the following: ε_∞, χ_{U1}, n, $f_{KWW} = (2\pi\tau)^{-1}$, β and the low-frequency limit of KWW relaxation, χ_{R0}. Good fitting to equation (3) was obtained in the whole frequency measurement range of 245–280 K and examples are shown in figure 8. At lower temperatures (e.g. 233 K) the dispersion related to one more relaxation process appeared at high frequencies (this behaviour was also observed in PMN) and the fitting was performed only in a narrower frequency range (after excluding the high-frequency data). However, by adding an additional term of the Cole–Cole form to relation (3) we were able to adequately describe the

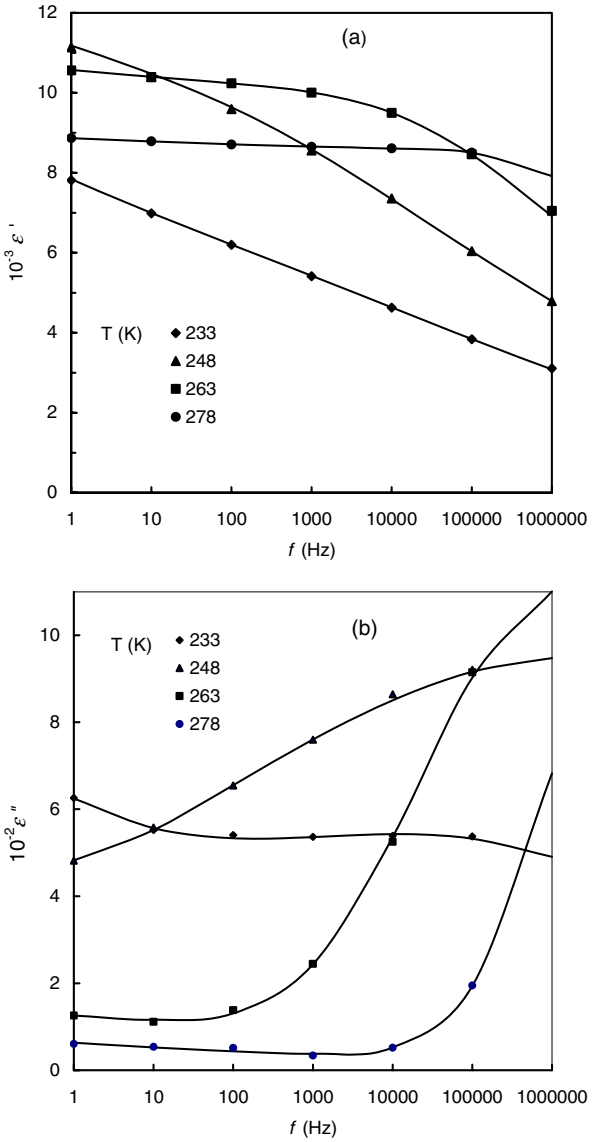

Figure 8. Fitting of the real (a) and imaginary (b) parts of permittivity at selected frequencies (solid lines). Experimental data are represented by dots.

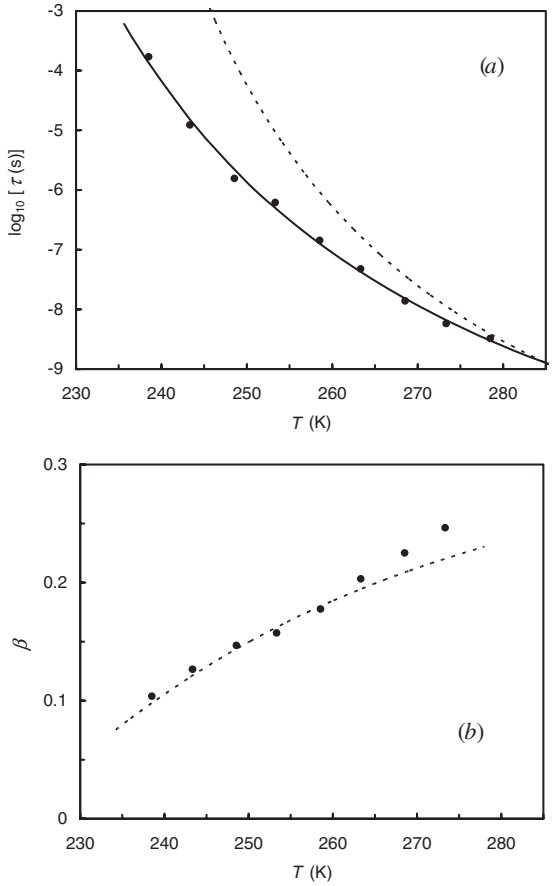

Figure 9. Temperature dependences of the characteristic time τ (a) and the KWW relaxation parameter β (b) of the PLMN crystal. The solid line is the fit to the Vögel–Fulcher relation (4). The dashed lines are the dependences for the pure PMN crystal taken from [26].

high-frequency part of the spectrum even at comparatively low temperatures, as shown in figure 8.

The temperature dependences of τ and β derived from fitting are shown in figure 9. These parameters determine the relaxation pattern of the CR dielectric contribution, which dominates in the temperature range of the permittivity peak. The corresponding temperature dependences for the pure PMN crystal are also given in figure 9 for comparison. One can see that the values of the parameters are close to each other. Similar to PMN, the temperature dependence of τ can be well fitted to the V–F relation,

$$\tau = (2\pi f_0^{-1}) \exp[E_a/(T - T_f)], \qquad (4)$$

and the best-fit parameters are presented in table 1. Fulfilment of the V–F relation (4) signifies the freezing of dipole dynamics in PLMN at the temperature T_f, which appears to be slightly lower than in PMN. The temperature dependences of the other relaxation parameters in PLMN also reveal behaviour similar to the case of PMN.

4. Discussion

According to the theoretical predictions [7, 8, 27], the dynamic PNRs (which are responsible for the large $\varepsilon'(T)$ peak and the dielectric dispersion in relaxors) should be strongly correlated with CORs so that '... within the range of $T_f < T < T_B$, polar nanoregions are essentially the same as chemically ordered nanoregions' [27]. Such a kind of correlation, even though true in pure PMN, is hardly compatible with the behaviour we have observed in PLMN. Indeed, the much larger size of PNRs in PLMN, as compared to PMN (caused by the much larger size of CORs), would imply a substantial difference in the dielectric relaxation parameters. However, the behaviour of the parameters derived from experimental data does not show any significant difference. In particular, the temperature dependences of τ and β, as well as the freezing temperature T_f, in PLMN and PMN are almost the same. Therefore, the characteristics of dynamic PNRs (particularly their size, which is expected to be roughly proportional to the activation energy of PNR flipping [7]) in PLMN and PMN should be close.

The molecular dynamic simulations [8, 27] predict the development of spontaneous polarization within the CORs (i.e. the formation of polar regions of the same size as CORs) upon cooling below a certain temperature. Therefore, in PLMN polar regions with dimensions of ∼100 nm are expected. These regions are large enough to be detected by x-ray diffraction as regions of (ferroelectric) rhombohedral phase. It seems that it is this phase that was found in our x-ray diffraction experiments, while the observed cubic phase can be attributed to the chemically disordered regions. To explain the dielectric behaviour in this case we use the concept recently proposed by Vakhrushev [28], who, based on the analysis of neutron and synchrotron radiation scattering data for PMN, suggested that PNRs which appear inside CORs are static while the dynamic PNRs are formed in the chemically disordered matrix. Static nanoregions should not contribute to the dielectric response, and their larger size in PLMN (as compared to PMN) should not influence directly the dielectric properties. On the other hand, the structure of the chemically disordered regions in PLMN is essentially the same as in PMN (except a small admixture of La). Therefore, the arrangement of the dynamic PNRs is expected to be similar. This explains why the experimentally determined dielectric relaxation parameters are close to each other. At the same time, the number of dynamic relaxing PNRs in PLMN is smaller than in PMN (because of the smaller fraction of the chemically disordered matrix) and consequently the level of the dielectric response (magnitude of the permittivity peak) is also smaller. The slightly lower freezing temperature T_f found in PLMN can be attributed to weaker interactions between dynamic PNRs caused by their lower overall concentration (the freezing temperature in the system of non-interacting dipoles should be zero).

5. Conclusions

High quality PMN and La-doped PMN single crystals with size up to 15 × 15 × 8 mm^3 were successfully grown by the top-seeded solution growth method. A-site La-doping at a level as low as 2 at.% is found to enhance the 1:1 B-site cation order significantly, and leads to the formation of the low-symmetry phase, which is presumably rhombohedral and mixed with the cubic phase. The strong chemical order was revealed by the presence of superlattice x-ray diffraction peaks and large ordered regions (∼100 nm) in the dark field images of transmission electron microscopy. The temperature dependence of ε' above T_m (and below T_B) can be well described by a Lorentz-type quadratic relationship characteristic of relaxors, with the diffuseness parameter δ being slightly larger in the PLMN crystal than in the pure PMN crystal. Analysis of the dielectric spectra of PLMN did not reveal any significant differences in comparison with PMN except the lower magnitude of the $\varepsilon'(T)$ peak. The glassy freezing of the main (CR) relaxation was found at T_f = 192 K. The relations between chemical and dipole orderings and between structure and properties are explained based on the concept of static and dynamic polar nanoregions.

Acknowledgments

The authors would like to thank Dr Weimin Zhu for help in structural simulation. This work was supported by the US Office of Naval Research (grant no. 00014-06-1-0166) and the National Science Foundation through the CAREER grant DMR-0346819.

References

[1] Smolensky G A 1970 *J. Phys. Soc. Japan* **28** 26
[2] Cross L E 1987 *Ferroelectrics* **76** 241
[3] Akbas M A and Davies P K 1998 *J. Am. Ceram. Soc.* **80** 2933
[4] Chen J, Chan H M and Harmer M P 1989 *J. Am. Ceram. Soc.* **72** 593
[5] Yan Y, Pennycook S J, Xu Z and Viehland D 1998 *Appl. Phys. Lett.* **72** 3145
[6] Xu Z, Kim M-C, Li J-F and Viehland D 1996 *Phil. Mag.* A **74** 395
[7] Randall C A and Bhalla A S 1990 *Japan. J. Appl. Phys.* **29** 327
Randall C A, Bhalla A S, Shrout T R and Cross L E 1990 *J. Mater. Res.* **5** 829
[8] Tinte S, Burton B P, Cockayne E and Waghmare U V 2006 *Phys. Rev. Lett.* **97** 137601
[9] Hilton A D, Barber D J, Randall C A and Shrout T R 1990 *J. Mater. Sci.* **25** 3461
Mathan N D, Husson E, Gaucher P and Morell A 1990 *Mater. Res. Bull.* **25** 427
[10] Akbas M A and Davies P K 2000 *J. Am. Ceram. Soc.* **83** 119
[11] Miao S, Zhu J, Zhang X W and Chen X H 2002 *J. Mater. Res.* **17** 2615
[12] Jiang F M, Kojima S, Zhao C L and Feng C D 2001 *Appl. Phys. Lett.* **79** 3938
[13] Miao S, Zhang X W and Zhu J 2001 *J. Am. Ceram. Soc.* **84** 2091
[14] Lee K M, Jang H M and Park W J 1997 *J. Mater. Res.* **12** 1603
[15] Montgomery J K, Akbas M A and Davies P K 1999 *J. Am. Ceram. Soc.* **82** 3481
[16] Davies P K and Akbas M A 2000 *J. Phys. Chem. Solids* **61** 159
[17] Qu W G, Zhao X H and Tan X L 2006 *Appl. Phys. Lett.* **89** 022904
[18] Zhao X H, Qu W G, He H, Vittayakorn N and Tan X L 2006 *J. Am. Ceram. Soc.* **89** 202
[19] Zhao X H, Qu W G, Tan X L, Bokov A A and Ye Z G 2007 *Phys. Rev.* B **75** 104106
[20] Fanning D M, Robinson I K, Jung S T, Colla E V, Viehland D D and Payne D A 2000 *J. Appl. Phys.* **87** 840
[21] Bokov A A and Ye Z-G 2006 *J. Mater. Sci.* **41** 31
[22] Bokov A A, Bing Y-H, Chen W, Ye Z-G, Bogatina S A, Raevski I P, Raevskaya S I and Sahkar E V 2003 *Phys. Rev.* B **68** 052102
[23] Bokov A A and Ye Z-G 2000 *Solid State Commun.* **116** 105
[24] Viehland D, Jang S G, Cross L E and Wutting M 1990 *J. Appl. Phys.* **68** 2916
[25] Glazounov A E and Tagantsev A K 1998 *Appl. Phys. Lett.* **73** 856
[26] Bokov A A and Ye Z-G 2006 *Phys. Rev.* B **74** 132102
[27] Burton B P, Cockayne E, Tinte S and Waghmare U V 2006 *Phase Transit.* **79** 91
[28] Vakhrushev S 2007 *Abstracts of 11th European Mtg on Ferroelectricity (Bled, Sept. 2007)* p 219